Hierarchical Porous Carbon Materials with High Capacitance Derived from Schiff-Base Networks

Ji-Shi Wei, Hui Ding, Yong-Gang Wang,* and Huan-Ming Xiong*

Department of Chemistry and Laboratory of Advanced Materials, Fudan University, Shanghai 200433, P. R. China

Ⓢ *Supporting Information*

ABSTRACT: A type of hierarchical porous carbon material was prepared using a Schiff-base network as the precursor and $ZnCl_2$ as the activation agent, and their electrochemical performances were investigated in acid and alkaline aqueous solutions, respectively. The as-prepared materials have high surface areas, appropriate distributions of hierarchical pore sizes, and various forms of nitrogen/oxygen derivatives. These structural advantages guarantee the outstanding performances of such carbon materials as electrodes for supercapacitors, which include high specific capacitances, fast current responses, and high cycling stabilities.

KEYWORDS: carbon materials, porous, dope, Schiff-base networks, supercapacitors
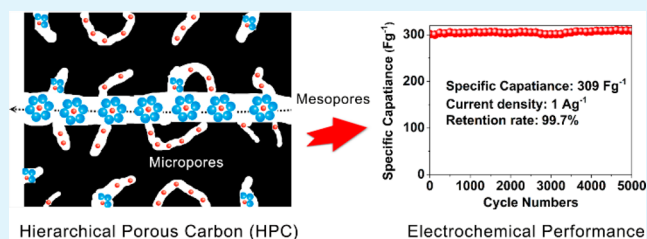
INTRODUCTION

Supercapacitors, as a type of energy storage device with distinguished performances in power density, cycle life, and cycle efficiency, have received intense attention in recent years.[1−6] The classical supercapacitors are electric double-layer capacitors (EDLCs) that store energy through reversible adsorption−desorption of electrolyte ions on the surface of active electrodes.[7] Because the capacitance of EDLCs is based on the total charges of the adsorbed ions, the specific surface areas (SSA) of the electrodes and the pore size distribution (PSD) on the electrode surfaces play the main roles in the design of electrode materials. It is interesting that the capacitance of the electrode materials usually increases with the SSA until some kind of saturation.[8,9] Such saturation is mainly caused by the sizes and structures of the pores on the electrode surfaces. In general,[10] micropores (diameter <2 nm) can enlarge the SSA to improve the EDLC effectively, mesopores (diameter = 2−50 nm) provide a low-resistant pathway for ions so as to improve the ion accessibility, and macropores (diameter > 50 nm) act as reservoirs for electrolyte ions to decrease the diffusion distances.[11−14] It has been found that too small pore sizes (diameter <0.5 nm) are usually inaccessible to electrolyte ions, and micropores with closed structures or narrow bottleneck morphologies often hinder ion transportation.[15,16] In fact, an appropriate proportion of micropores to mesopores is beneficial to both the energy and power densities of EDLCs. Besides, adaptation between the pore sizes and ion diameters is also important for EDLCs. As suggested by Gogotsi et al., when the pore sizes match the diameters of the electrolyte ions and their solvation shells, desolvation takes place as the ions enter the micropores, which shortens the distances between the electrolyte ions on the electrode surfaces and thus improves the capacitance of the electrodes anomalously.[1,3] Therefore, a facile way of constructing appropriate hierarchical pore structures for electrode materials is desired in practical researches.

Besides the SSA and PSD, pseudocapacitance also contributes to the specific capacitance. For example, introducing heteroelements like nitrogen onto carbon electrode surfaces is an effective way to improve the specific capacitance because of the extra faradaic redox reactions and improved surface wettability.[8,14,17−22] After post-treatment on products with ammonia, amine, urea, or pyridine or the direct use nitrogen-related precursors like polyaniline,[17] polypyrrole,[18] and polyacrylonitrile,[19,20] various nitrogen derivatives will form in carbon materials. Among them, pyrrolic/pyridonic-type nitrogen (N-5) and pyridine-type nitrogen (N-6) contribute to the pseudocapacitance,[23] while quaternary-type nitrogen (N-Q) and oxidized nitrogen (N-X) promote electron transport.[7] Recently, Feng's group used aminated graphene oxide and a porous Schiff-base polymer to prepare a kind of nitrogen-rich electrode material that exhibited an ultrahigh capacitance of 424 F g^{-1} at a current density of 0.1 A g^{-1} in a 6 mol L^{-1} KOH solution.[24] Such a Schiff-base network (SNW) material has many advantages over conventional nitrogen-rich precursors because of its rigid molecular backbone and high nitrogen content, and it does not need expensive transition-metal catalysts for preparation. However, the above work required 3 days for the complicated preparation and a high reaction temperature of 180 °C,[25] with a yield of 70−90%. Other groups employed ultrasonication and microwave to synthesize SNW materials in a short time successfully,[26,27] but the results were not ideal.

Scheme 1. Synthetic Route of the HPC Materials
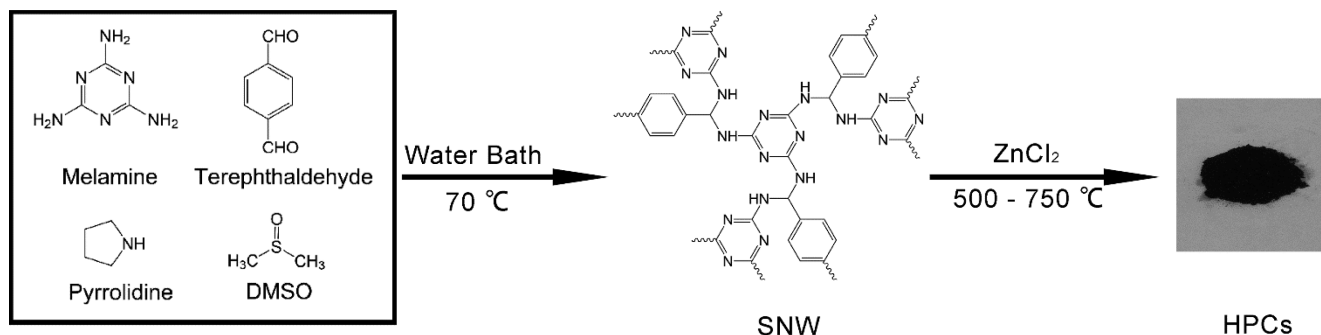
In the present work, we first used pyrrolidine as a catalyst to obtain melamine-based SNW materials with a high yield of about 95% under mild conditions in a short time.[28] After that, the SNW was calcined with ZnCl₂ to prepare activated porous carbon. The high surface area, appropriate nitrogen/oxygen ratio, and desirable hierarchical porous structure of the final products were realized by adjusting the ZnCl₂ ratio and calcination temperature. The electrochemical measurements on the optimal carbon material in acidic and basic aqueous solutions showed much better performances than those results in the previous work by our group and other researchers.[2,7,16,24,29−31]

EXPERIMENTAL SECTION

Materials. Pyrrolidine (C_4H_9N, 99.0%) was from Aladdin Corp. Activated carbon (QHA-325; $S_{BET} \approx 1000$ m² g⁻¹) was from Shanghai Quanhu Active Carbon Co. Ltd. Melamine, terephthaldehyde, dimethyl sulfoxide, zinc chloride ($ZnCl_2$), sulfuric acid, dichloromethane, acetone, tetrahydrofuran, and other chemicals were from Shanghai Chemical Corp. All chemicals were used as received.

Synthesis of SNW. A microreaction vessel (10 mL) was filled with melamine (121.2 mg), terephthalaldehyde (193.5 mg), dimethyl sulfoxide (6.0 mL), and pyrrolidine (603 mg). The reaction mixture was degassed by nitrogen for 10 min, and then the vessel was sealed and heated to 70 °C in a water bath for 12 h. After cooling to room temperature, the resulting polymer precipitates were separated by filtration and washed thoroughly with acetone, tetrahydrofuran, dichloromethane, and deionized water consecutively. The precipitates were further dried in a vacuum at 100 °C for 24 h. The product (SNW) was an off-white powder with a yield of about 95%.

Synthesis of Nitrogen-Rich Porous Carbon. The obtained SNW was mixed with a ZnCl₂ aqueous solution (40 wt %) by different mass ratios of SNW/ZnCl₂ (1:2, 1:3, and 1:4) for 12 h. Afterward, the mixture was dried in a vacuum at 80 °C for 12 h. The impregnated material was heated to 300 °C at a rate of 5 °C min⁻¹ in a tube furnace, and then maintained at 300 °C for 1 h. Thereafter, the temperature was raised to 500, 550, 600, 650, 700, and 750 °C at a rate of 2 °C min⁻¹ and maintained at the desired temperature for 2 h. The whole process was under a nitrogen atmosphere with a flow rate of 60 mL min⁻¹. The products were first washed with a 1 mol L⁻¹ HCl solution to remove inorganic salts and then washed with distilled water repeatedly. Finally, the products were dried in a vacuum oven at 80 °C for 24 h, and the obtained yields varied from 66% to 77%.

Structural Characterization. The X-ray diffraction (XRD) patterns were collected at room temperature using a Bruker D4 Endeavor X-ray diffractometer with Cu Kα radiation (λ = 0.1541 nm, 40 kV). Fourier transform infrared (FTIR) spectra were recorded on a PerkinElmer Avatar 360 ESP FTIR spectrometer in a range of 4000−400 cm⁻¹, using the KBr pellet method. Nitrogen adsorption−desorption measurements were performed at 77.3 K with a Quantachrome Autosorb SI surface area analyzer to obtain the SSA, total pore volume, PSD, etc. X-ray photoelectron spectroscopy (XPS) data were obtained by a Thermo ESCALAB 250 electron spectrometer

using an Al Kα X-ray source (1486.6 eV). The morphologies of the samples were characterized via scanning electron microscopy (SEM) under a JSM-6390 microscope, while the transmission electron microscopy (TEM) images of the samples were obtained by a high-resolution transmission electron microscope (JEM-2010) at 200 kV.

Electrochemical Measurements. Cyclic voltammetry (CV), the galvanostatic charge−discharge (GCD) profile, and electrochemical impedance spectroscopy (EIS) of the SNW-based carbon materials were measured in 1 mol L⁻¹ H_2SO_4 and 6 mol L⁻¹ KOH aqueous solutions. CV was recorded on a CH Instruments 660E electrochemical workstation at the potential range of −0.8 to +0.2 V in H_2SO_4 and −1 to 0 V in KOH, and the scan rate was set from 2 to 200 mV s⁻¹. GCD tests were performed by a CT2001A Land cell tester at the same potential ranges, while the current densities varied from 0.2 to 30 A g⁻¹. EIS measurements were also conducted on the CHI660E electrochemical workstation in two electrolytes, in which the frequency limits were set at 100 kHz to 0.01 Hz with 5 mV of voltage amplitude at the open-circuit potential. All electrochemical measurements were carried out with a three-electrode system. The working electrode was prepared by pressing a mixture of the sample (75 wt %), acetylene black (20 wt %), and poly(tetrafluoroethylene) (PTFE) binder (5 wt %) onto a stainless steel grid with an area of 1 cm², followed by drying at 80 °C for 24 h, and the active material loading for each electrode was 1.2 mg cm⁻². The counter electrode was prepared with activated carbon, acetylene black, and PTFE binder in the same method, but the area of the counter electrode was about 3 cm². Hg/Hg₂SO₄ (in a saturated K₂SO₄ solution) and Hg/HgO (in a 1 mol L⁻¹ KOH solution) were chosen as the reference electrodes for the H₂SO₄ and KOH electrolytes, respectively.

RESULTS AND DISCUSSION

In the preparation of the precursor, pyrrolidine plays an important role. Pyrrolidine and terephthalaldehyde will format the C═N⁺ intermediate at first, and this important intermediate will rapidly promote the reaction between the primary amine and aldehyde (see Scheme S1 in the Supporting Information, SI).[25,28] Scheme 1 illustrates the preparation process of the hierarchical porous carbon (HPC) powder. These products are denoted as HPCX-Y, in which X represents the mass ratio of ZnCl₂ versus SNW precursor while Y represents the carbonization temperature. Through preliminary charge−discharge tests, as shown in Table S1 in the SI, the HPC3-Y samples show better performances in both specific capacitances and rate capabilities. At the same time, the electrochemical performance between carbon materials prepared with pyrrolidine and materials prepared without pyrrolidine were compared by CV (see Figure S1 in the SI). There is no obvious difference, which proves that pyrrolidine just plays an efficient catalyst in the preparation of SNW. After the preparative conditions were optimized, we obtained HPC3-600 with the best performances, which involved its SSA, PSD, surface elements, and electrochemical properties.

Structure and Morphology. The FTIR spectra of SNW and HPC3-600 are compared in Figure 1. For SNW, the
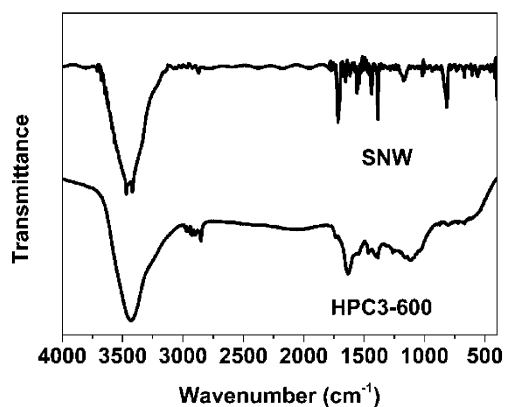

Figure 1. FTIR spectra of SNW and HPC3-600.

vibration bands at 3470 and 3420 cm^{-1} are ascribed to the NH$_2$ stretching of the melamine groups, while the vibration bands at 1548 and 1450 cm^{-1} are due to the triazine rings.[26] In the meantime, the −NH− and NH$_2$− stretching vibrations of the secondary amine (C−N) are observed at 1384, 1170, and 814 cm^{-1}. The absence of the C=O stretching band at 1715 cm^{-1} and the C−H stretching band at 2870 cm^{-1}, corresponding to the carbonyl function of aldehydes, confirms the formation of SNW. In addition, there are no FTIR bands corresponding to the imine linkage stretching vibration around 1600 cm^{-1} for the SNW.[24−27,32] After chemical activation and pyrolysis, many fine FTIR structures of the original SNW disappear in HPC3-600. For example, the original bands at 3470 and 3420 cm^{-1} in the SNW are replaced by a broad band at 3436 cm^{-1}, indicating that the N−H and O−H stretching peaks cannot be distinguished in HPC3-600. Nevertheless, the three-dimensional (3D) network structure of a SNW containing a triazine ring, a benzene ring, and C−N bonds remains in HPC3-600, which is evidenced by FTIR bands at about 1450 and 1384 cm^{-1}.

The XRD patterns of HPC3-600 are shown in Figure 2, which consist of three broad diffraction peaks with 2θ values of
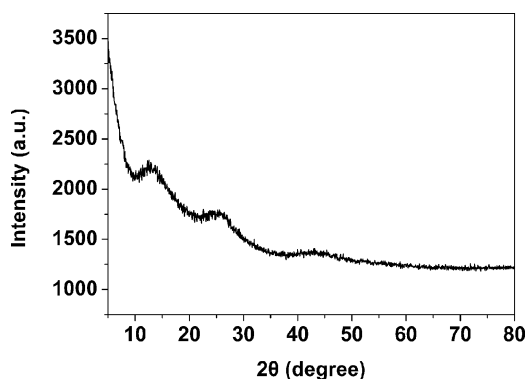

Figure 2. XRD patterns of HPC3-600.

about 12°, 23.5°, and 43.5° corresponding to the (001) plane of graphite oxide[33,34] and the (002) and (101) planes of graphitic carbon materials, respectively.[35] For a typical graphite oxide, the (001) diffraction is at 13.3° and the corresponding d spacing is 0.67 nm.[36] According to the Bragg equation, the d

spacing of HPC3-600 is larger than 0.67 nm, which can be ascribed to the intercalation of water and functional groups.[33]

The porous features of HPC3-600 are evaluated by nitrogen physisorption measurements at 77.3 K, and the specific results are shown in Figure 3 and Table 1. The nitrogen adsorption
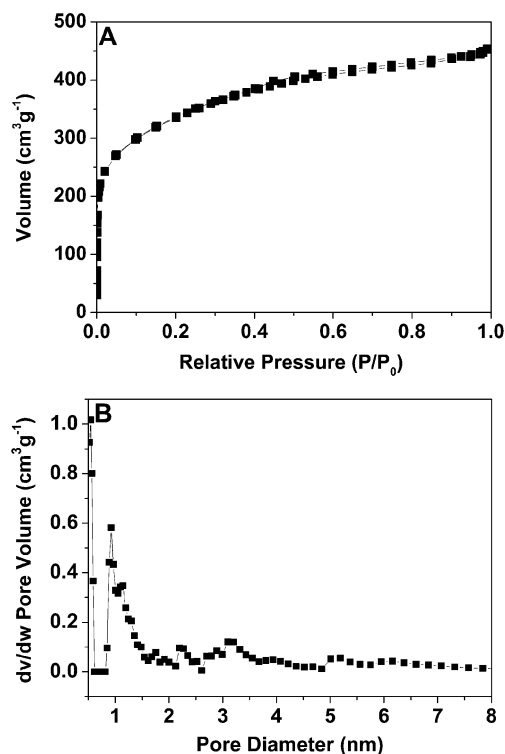

Figure 3. (A) Nitrogen adsorption−desorption isotherms and (B) PSD calculated by the DFT method of HPC3-600.

Table 1. Porosity Properties of HPC3-600[a]

S_{BET} (m^2 g^{-1})	S_{micro} (m^2 g^{-1})	V_{tot} (cm^3 g^{-1})	V_{micro} (cm^3 g^{-1})	S_{micro}/S_{BET} (%)	V_{micro}/V_{meso}
1203.43	912.9	0.641	0.338	75.86	1.12

[a]Its micropore sizes are 0.55, 0.93, 1.14, 1.76, and 1.92 nm, while its mesopore sizes are 2.2, 2.9, 3.1, 5.2, and 6.2 nm. The micropore and mesopore volumes are derived from DFT.

isotherm curve for HPC3-600 belongs to type I, which exhibits distinct H4-type hysteresis loops at relative pressures of 0.4−1.0, indicating that the systems are composed of slitlike micro/mesopores and the dominant pores are micropores. The results obtained from the density functional theory (DFT) method demonstrate that the material has a hierarchical pore construction assembled by micropores and mesopores. Müllen et al.[25] reported that the Brunauer−Emmett−Teller (BET) surface area of SNW was 1377 m^2 g^{-1} but decreased to 382 m^2 g^{-1} after pyrolysis at 450 °C. In our present work, the surface area of the calcined HPC3-600 is up to 1203 m^2 g^{-1} by ZnCl$_2$ activation. Hence, ZnCl$_2$ plays an important role in the evolvement of both the pore volume and pore type. It acts as a dehydration reagent and a template simultaneously during the activation process and influences aromatization of the carbon skeleton and the creation of porosity.[37]

Besides the surface area, an adequate PSD in the electrode materials is also important for obtaining high capacitance, which includes a balance between the micro-, meso-, and

macroporosities as well as a match between the pores and electrolyte ions. In the present HPC3-600, many pores have diameters in the range of 0.5−1 nm, which are suitable for the solvated SO_4^{2-}, K^+, and H_3O^+ ions[10,15] and contribute greatly to the specific capacitance. Our HPC3-600 also has pores with diameters in the range of 1.2−7 nm, which exhibit excellent ion accessibility.[12] In addition, the annealing temperature is another critical factor. Optimal gravimetric capacitance values are obtained for materials calcined at 600 °C (see Tables S5 and S6 in the SI) because a suitable calcination process can produce an additional pseudocapacitance that is based on high contents of pyridinic nitrogen and pyrrolic nitrogen and oxygen species.[8]

XPS was employed to study the oxygen and nitrogen species on the HPC3-600 surface. The broad scan of XPS (Figure 4)
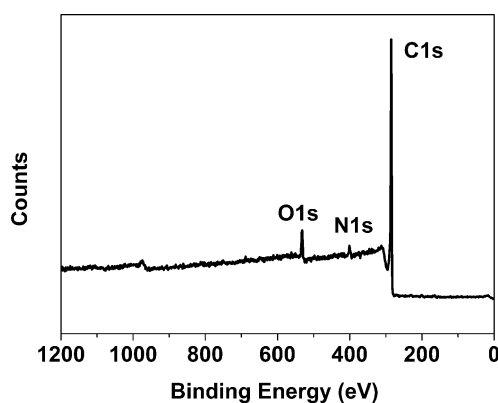
Figure 5. High-resolution XPS of N 1s (A) and O 1s (B) of HPC3-600.

Figure 4. XPS survey spectra of HPC3-600.

confirms the presence of carbon, nitrogen, and oxygen in HPC3-600, while zinc and chlorine residues are not found. It is known that $ZnCl_2$ activation can increase the content of surface oxygen species and change the whole element distribution.[38] In the meantime, nitrogen species are also influenced by chemical activation and calcination. In Figure 5, the N 1s spectra can be deconvoluted into four peaks corresponding to N-6 (pyridine-type nitrogen; BE = 398.5 eV), N-5 (pyrrolic and pyridonic-type nitrogen or amine moieties; BE = 400.3 eV), N-Q (quaternary-type nitrogen; BE = 401.1 eV), and N-X (oxidized nitrogen; BE = 403 eV).[39,40] The O 1s spectra can be deconvoluted into different species, such as C=O groups or quinone (BE = 530.5−531 eV), C−OH groups and/or phenol (BE = 532 eV), C−O−C groups (BE = 533.5 eV), COOH carboxyl groups and/or water (BE = 534.5 eV), etc.[23,38]

In Table 2, the atomic proportions of nitrogen and oxygen are 2.73% and 5.36%, respectively. As previously described, N-6 and N-5 species contribute to the pseudocapacitance, while N-Q and N-X species facilitate electron transport.[7] The former has a content close to that of the latter, indicating that HPC3-600 will have both a high pseudocapacitance and a good conductivity. In contrast, the oxygen-related functional groups can also increase the pseudocapacitance, but an excess of them has a negative impact on the electrical conductance.[41] Therefore, tuning the contents of nitrogen and oxygen species by calcination is important to the whole performance of the product, and 600 °C calcination with $ZnCl_2$ was found as the optimal condition (see Table S3 in the SI).

The morphology of HPC3-600 was examined by SEM and TEM. Although the SEM results show that the samples are disordered (see Figure S6 in the SI), the TEM image in Figure 6 shows the material has graphitic (002) layers, graphite
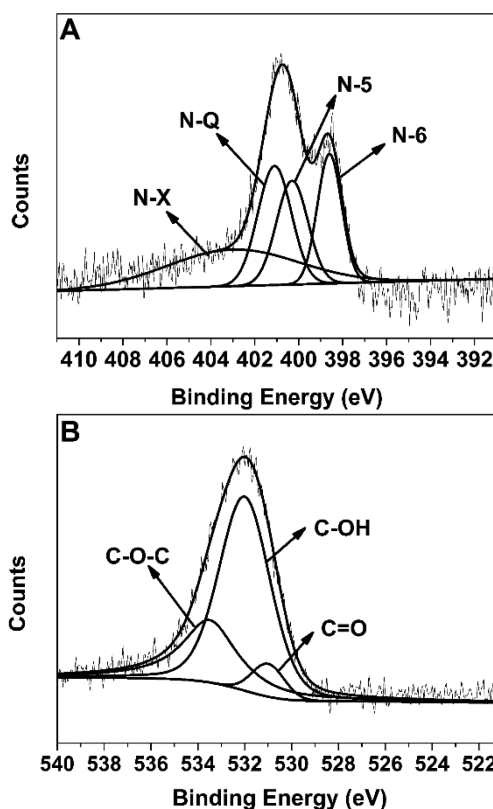
ribbons, and random micropores. Selected-area electron diffraction (SAED) confirms that the products are noncrystalline materials, which is in agreement with XRD analyses.

Electrochemical Measurements. Chemical activation and carbonation can produce oxygen-related functional groups, such as C−OH, C=O, and −COOH, on the surface of the carbon material, and these groups are able to enhance the pseudocapacitance. In a KOH medium, some redox reactions are considered, as in Scheme 2.[42]

It should be noted that the above reactions are quasi-reversible, especially in a KOH medium, and after a long cycling, the pseudocapacitance will decrease gradually.[43] At the same time, other reactions may also occur in the carbon negative electrode.[44] For example, K^+ ions can be inserted into the lattice of porous carbons to provide extra capacitance, as in Scheme 3.

It should be mentioned that the underpotential hydrogen adsorption−desorption may have occurred at −1 V versus Hg/HgO by the following reaction, in which water is reduced to hydrogen atoms. Thus, the electrode performances in the KOH electrolyte are generally worse than those in a H_2SO_4 solution.

In a H_2SO_4 solution, some oxygen-related groups like carbonyl and quinone play important roles in the pseudocapacitance (Scheme 4).[45]

Besides the oxygen-related functional groups, nitrogen-related species like pyrrolic and pyridinic groups also contribute to the capacitance in the faradaic reactions in Schemes 5 and 6.[8,23,46−48]

These oxygen/nitrogen derivatives exit on the surfaces of HPC3-600, as proven by XPS and FTIR data, which determine the pseudocapacitance behaviors in electrolytes. The CV performances of HPC3-600 in 6 mol L^{-1} KOH and 1 mol

Table 2. Surface Atomic Percentages of Nitrogen and Oxygen Species Obtained from XPS Analyses

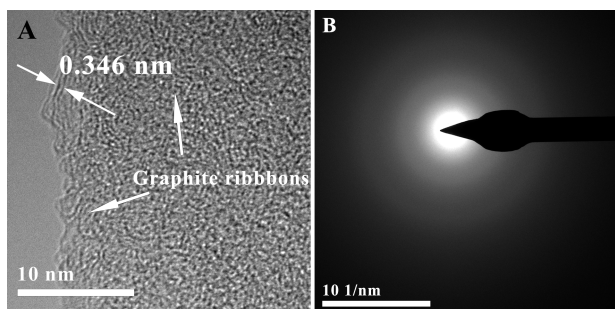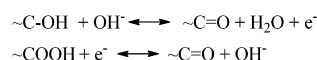| sample	species concentration (%)			N 1s %					O 1s %		
	C 1s	N 1s	O 1s	N-5	N-6	N-Q	N-X	N-5 + N-6	C=O	C−OH	C−O−C
HPC3-600	91.8	2.73	5.46	0.80	0.64	0.66	0.64	1.44	0.34	3.50	1.62

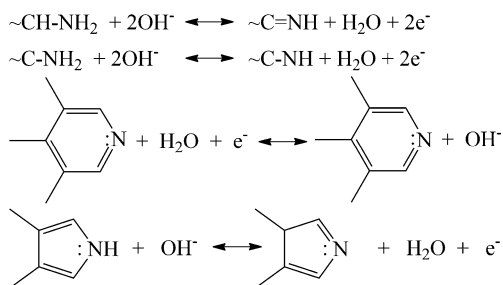**Figure 6.** (A) TEM image and (B) the corresponding SAED pattern of HPC3-600.

Scheme 2. Reactions of Oxygen-Related Functional Groups under Alkaline Conditions

$$\sim\!C\text{-}OH + OH^- \longleftrightarrow \sim\!C\!=\!O + H_2O + e^-$$
$$\sim\!COOH + e^- \longleftrightarrow \sim\!C\!=\!O + OH^-$$

Scheme 3. K$^+$ Ions Inserted into the Lattice of Porous Carbons

$$\sim\!CO^- + K^+ \longleftrightarrow \sim\!CO^- \| K^+$$
$$\sim\!CO + K^+ + e^- \longleftrightarrow \sim\!COK$$
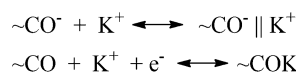
Scheme 4. Reactions of Oxygen-Related Functional Groups under Acidic Conditions

$$\sim\!C\!=\!O + H^+ + e^- \longleftrightarrow \sim\!CH\text{-}O$$
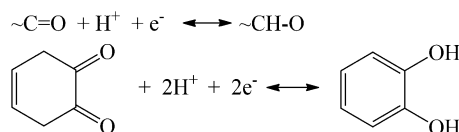
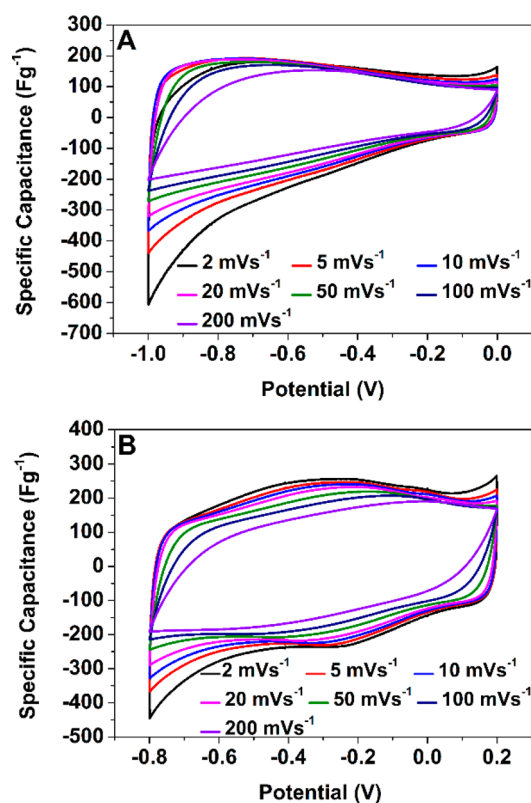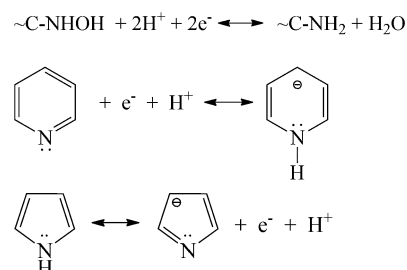**Scheme 5. Reactions of Nitrogen-Related Functional Groups under Alkaline Conditions in a Basic Aqueous Electrolyte**

$$\sim\!CH\text{-}NH_2 + 2OH^- \longleftrightarrow \sim\!C\!=\!NH + H_2O + 2e^-$$
$$\sim\!C\text{-}NH_2 + 2OH^- \longleftrightarrow \sim\!C\text{-}NH + H_2O + 2e^-$$

Scheme 6. Reactions of Nitrogen-Related Functional Groups under Acidic Conditions in an Acidic Aqueous Electrolyte

$$\sim\!C\text{-}NHOH + 2H^+ + 2e^- \longleftrightarrow \sim\!C\text{-}NH_2 + H_2O$$

**Figure 7.** CV curves of HPC3-600 at different scan rates from 2 to 200 mV s^{-1} in (A) a KOH solution and (B) a H$_2$SO$_4$ solution.

L^{-1} H$_2$SO$_4$ aqueous electrolytes are evaluated using a three-electrode system. The profiles in the potential range of −1 to 0 V versus Hg/HgO in a KOH solution are recorded in Figure 7A, while the profiles in the potential range of −0.8 to +0.2 V versus a Hg/Hg$_2$SO$_4$ electrode in a H$_2$SO$_4$ solution are recorded in Figure 7B. The CV shape in the KOH solution is asymmetric, indicating that the reversibility and capacitance performance of the material are not ideal because hydrogen evolution can take place at low potentials in basic electrolytes. In contrast, the shape of the CV curves in H$_2$SO$_4$ solution is almost square, indicating ideal capacitance behavior based on electrostatic attraction. A pair of symmetrical, wide-redox peaks are observed in these curves, which is the character of the faradaic pseudocapacitance. These results are consistent with the GCD data in the SI (see Tables S5 and S6). Nevertheless, in both KOH and H$_2$SO$_4$ solutions, the nearly 90° turnings in all of the CV curves at the switching potentials indicate that HPC3-600 has a very fast response as an ideal capacitor material.

EIS was employed to study the capacitance of HPC3-600 in another way. In a typical Nyquist impedance plot like Figure 8A, the semicircle at the high-frequency region represents the conductivity of the active materials and electrolyte, the high-to-
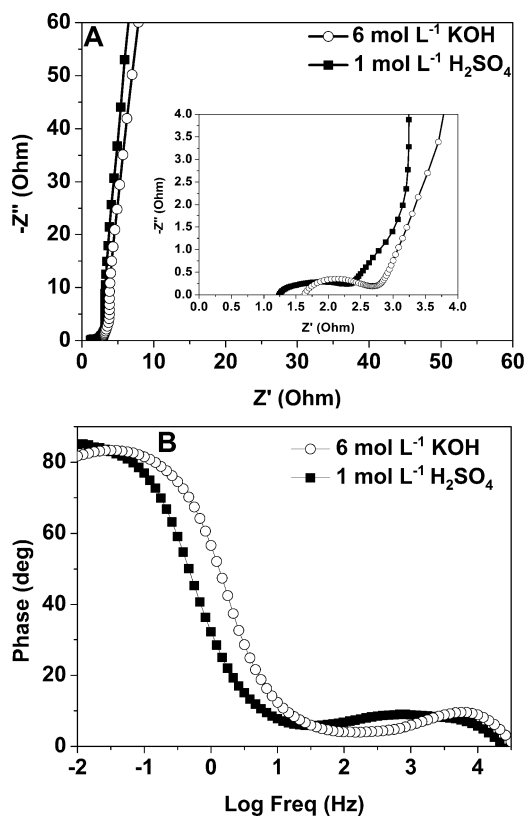
Figure 8. (A) Nyquist impedance plots of HPC3-600 carbons in KOH and H_2SO_4 solutions at the open-circuit potential. (B) Bode plots of HPC3-600 in KOH and H_2SO_4 solutions.

Figure 9. GCD curves of HPC3-600 (A) in KOH solutions with current densities of 1, 2, 5, 10, 20, and 30 A g^{-1} and (B) in H_2SO_4 solutions with current densities of 0.2, 0.3, 0.4, 0.5, 1, 2, 5, 10, 20, and 30 A g^{-1}.

medium-frequency region shows the pseudo-charge-transfer resistance that is related to the structure of the porous carbon electrodes, and the nearly vertical line along the imaginary axis at the low-frequency region is associated with the feature of the capacitive behavior.[49] At the high- and medium-frequency region, as shown in the inset of Figure 8A, after the semicircles are extended to intersect with the X axis, the fitted radius of the semicircle is regarded as the internal contact resistance of the electrode (R_{ct}). The fitted values are 1.15 and 1.27 Ω for the samples in KOH and H_2SO_4 solutions, respectively. These values are relatively less than those of other nitrogen- or oxygen-doped porous carbon materials.[2,7,29] In our HPC3-600 sample, on the one hand, the high contents of N-Q and N-X species promote electron transport, and, on the other hand, an appropriate concentration of mesopores contributes to the ion accessibility, and thus HPC3-600 exhibits an ideal electrode resistance. It is known that the Nyquist plot at the low-frequency region is a vertical line for an ideal electrode material, and the more vertical the line, the better capacitive performance it shows.[50] In comparison with the result in a H_2SO_4 solution, the slope of the line obtained in a KOH solution is obviously smaller, and thus the material exhibits better capacitor properties in a H_2SO_4 solution. The Bode plots in Figure 8B show that the phase angles of both curves are close to 90°, indicating that the capacitor behaviors are almost perfect.

GCD tests were used to investigate the electrochemical capacitive performances of HPC3-600, as shown in Figure 9. In a H_2SO_4 solution, the GCD curves exhibit typical triangular shapes between −0.8 and +0.2 V versus Hg/Hg_2SO_4 (Figure 9A) without any obvious ohmic drop, and the optimal capacitance reached 377 F g^{-1} at 0.2 A g^{-1}. However, the
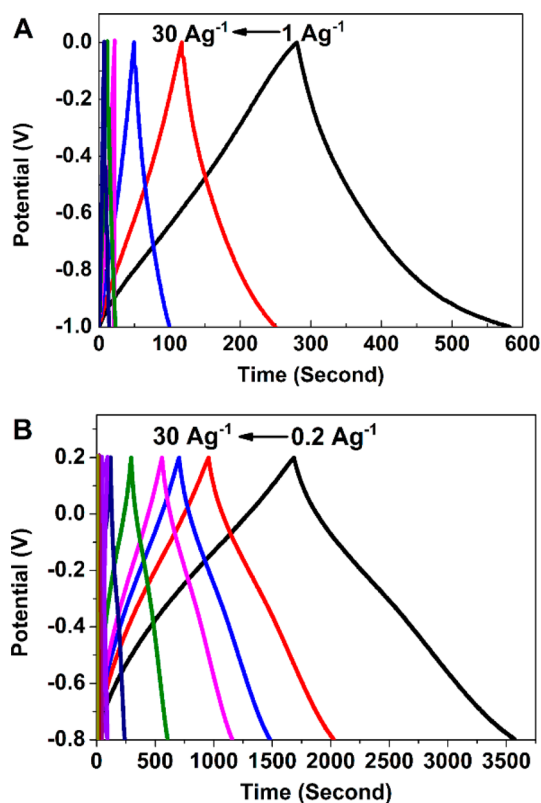
GCD curves in a KOH solution show a slight degree of deviation from the lines at the lower potential, especially at the current density of 1 A g^{-1}. When the current density is less than 1 A g^{-1}, a degree of hydrogen evolution phenomenon will occur. This result demonstrates that nitrogen-rich carbon materials have better capacitive performances in an acidic medium.[8,51]

The specific capacitance (C_m) of the working electrode is calculated by the equation[17] $C_m = It/m\Delta V$. Figure 10 shows variation of the specific capacitance for HPC3-600 at current densities of 1, 2, 5, 10, 20, and 30 A g^{-1} in two different solutions. The capacitance of HPC3-600 in a H_2SO_4 solution
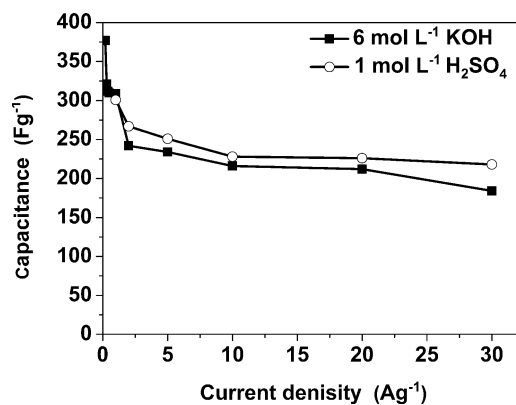
Figure 10. Rate performances of HPC3-600 at different current densities in H_2SO_4 and KOH solutions, respectively.

drops sharply at low current densities (0.2−2 A g^{-1}) and then declines slower at higher current densities (5−30 A g^{-1}). The situations are similar in a KOH solution. When the current density varies from 1 to 30 A g^{-1}, the retention rates reach 59.5% and 72.4% in H$_2$SO$_4$ and KOH media, respectively.

Figure 11 shows the cycling performance of HPC3-600 at various current densities in two electrolytes. Obviously, the
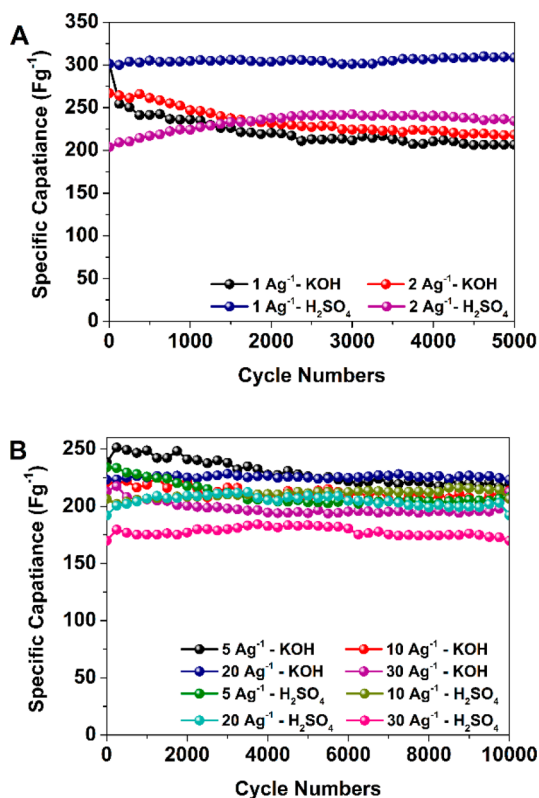
Figure 11. Cycle stability of HPC3-600 at current densities of (A) 1 and 2 A g^{-1} and (B) 5, 10, 20, and 30 A g^{-1} in two different electrolytes, respectively.

stability of the electrode material in acidic conditions is better than that in alkaline conditions. In a H$_2$SO$_4$ solution, after 5000 or 10000 cycles, the capacity decay is only 0.3% at 1 A g^{-1}, 3% at 2 A g^{-1}, and 7.7% at 30 A g^{-1}, indicating the excellent cycle durability of HPC3-600. The slight increase of the capacitance with the cycle number is usually caused by continuous penetration of the electrolyte into the porous carbon electrode materials.[2] In contrast, the stability of the HPC3-600 capacity in a KOH solution performs less well especially at low current densities (1 and 2 A g^{-1}), which is ascribed to those quasi-reversible reactions mentioned above. However, at high current densities, HPC3-600 still exhibits good electrochemical stability in a KOH solution. Besides, HPC3-600 also presents good reproducibility in two different electrolytes, the relative average deviation values of which are between 0.2% and 1.4% (see Tables S7 and S8 in the SI). Both the specific capacitance and cycle stability are superior over other porous carbon materials that are derived from many precursors, such as quinoline-polymerized pitch,[2] soluble phenolic resole,[7] melamine,[23,30,52−55] terephthalonitrile,[31] and biomass[35,52] (see Table S9 in the SI).

CONCLUSIONS

Our present work develops a facile high-yield synthetic method for a type of porous nitrogen-doped carbon material using pyrrolidine as the catalyzer and ZnCl$_2$ as the activation agent. These SNW-based carbon materials possess high surface areas, appropriate PSDs, hierarchical porous structures, and high nitrogen/oxygen contents. The optimal material HPC3-600 exhibits distinguished electrochemical performances, including a capacitance up to 377 F g^{-1} at 0.2 A g^{-1} and a capacitance retention of 99.7% at 1 A g^{-1} over 5000 cycles in a 1 mol L^{-1} H$_2$SO$_4$ aqueous electrolyte. Such outstanding performances are ascribed to three merits of our carbon materials.[56] First, a suitable hierarchical pore distribution and a large SSA (1203 m^2 g^{-1}) provide efficient spaces for storage of ions and short distances for ion transport and thus make a great contribution to the EDLC. Second, nitrogen and oxygen heteroatoms are able to induce faradaic reactions, enhance the surface compatibility with aqueous electrolytes, and provide low-resistance pathways for ions. Third, the 3D cross-linked structure combined with the 3D interconnected pore texture offers good charge accommodation and excellent adaption for repeated charging−discharging. Therefore, such porous carbon materials will have potential applications not only in electro-chemical energy storage but also in electrochemical catalysis.

ASSOCIATED CONTENT

S Supporting Information

Experimental details and comparable data. This material is available free of charge via the Internet at http://pubs.acs.org.

AUTHOR INFORMATION

Corresponding Authors
*E-mail: ygwang@fudan.edu.cn.
*E-mail: hmxiong@fudan.edu.cn.
Notes
The authors declare no competing financial interest.

ACKNOWLEDGMENTS

REFERENCES

(1) Chmiola, J.; Yushin, G.; Gogotsi, Y.; Portet, C.; Simon, P.; Taerna, P. L. Anomalous Increase in Carbon Capacitance at Pore Sizes Less Than 1 Nanometer. *Science* **2006**, *313*, 1760−1763.

(2) Song, Y. F.; Zhou, D. D.; Wang, Y. G.; Wang, C. X.; Xia, Y. Y. Preparation of Nitrogen-Containing Mesoporous Carbons and Their Application in Supercapacitors. *New J. Chem.* **2013**, *37*, 1768−1775.

(3) Wang, Y. G.; Xia, Y. Y. Recent Progress in Supercapacitors: From Materials Design to System Construction. *Adv. Mater.* **2013**, *25*, 5336−5342.

(4) Zhang, L. J.; Wang, J.; Zhu, J. J.; Zhang, X. G.; Hui, K. S.; Hui, K. N. 3D Porous Layered Double Hydroxides Grown on Graphene as Advanced Electrochemical Pseudocapacitor Materials. *J. Mater. Chem. A* **2013**, *1*, 9046−9053.

(5) Yang, J.; Xiong, P. X.; Zheng, C.; Qiu, H. Y.; Wei, M. D. Metal−Organic Frameworks: A New Promising Class of Materials for A High Performance Supercapacitor Electrode. *J. Mater. Chem. A* **2014**, *2*, 16640−16644.

(6) Mai, L. Q.; Minhas-Khan, A.; Tian, X. C.; Hercule, K. M.; Zhao, Y. L.; Lin, X.; Xu, X. Synergistic Interaction between Redox-Active

Electrolyte and Binder-Free Functionalized Carbon for Ultrahigh Supercapacitor Performance. *Nat. Commun.* **2013**, *4*, 2923.

(7) Zhou, D. D.; Li, W. Y.; Dong, X. L.; Wang, Y. G.; Wang, C. X.; Xia, Y. Y. A Nitrogen-doped Ordered Mesoporous Carbon Nanofiber Array for Supercapacitors. *J. Mater. Chem. A* **2013**, *1*, 8488–8496.

(8) Frackowiak, E. Carbon Materials for Supercapacitor Application. *Phys. Chem. Chem. Phys.* **2007**, *9*, 1774–1785.

(9) Wang, L. H.; Toyoda, M.; Inagaki, M. Dependence of Electric Double Layer Capacitance of Activated Carbons on the Types of Pores and Their Surface Areas. *New Carbon Mater.* **2008**, *23*, 111–115.

(10) Inagaki, M. Pores in Carbon Materials—Importance of Their Control. *New Carbon Mater.* **2009**, *24*, 193–232.

(11) Cheng, Q. L.; Xia, Y. M.; Pavlinek, V.; Yan, Y. F.; Li, C. Z.; Saha, P. Effects of Macropore Size on Structural and Electrochemical Properties of Hierarchical Porous Carbons. *J. Mater. Sci.* **2012**, *47*, 6444–6450.

(12) Kumagai, S.; Sato, M.; Tashima, D. Electrical Double-Layer Capacitance of Micro- and Mesoporous Activated Carbon Prepared from Rice Husk and Beet Sugar. *Electrochim. Acta* **2013**, *114*, 617–626.

(13) Wang, K. X.; Wang, Y. G.; Wang, Y. R.; Hosono, E.; Zhou, H. S. Mesoporous Carbon Nanofibers for Supercapacitor Application. *J. Phys. Chem. C* **2009**, *113*, 1093–1097.

(14) Hulicova, D.; Yamashita, J.; Soneda, Y.; Hatori, H.; Kodama, M. Supercapacitors Prepared from Melamine-Based Carbon. *Chem. Mater.* **2005**, *17*, 1241–1247.

(15) Hulicova, D.; Kodama, M.; Hatori, H. Electrochemical Performance of Nitrogen-Enriched Carbons in Aqueous and Non-Aqueous Supercapacitors. *Chem. Mater.* **2006**, *18*, 2318–2326.

(16) Liu, H. J.; Wang, J.; Wang, C. X.; Xia, Y. Y. Ordered Hierarchical Mesoporous/Microporous Carbon Derived from Mesoporous Titanium-Carbide/Carbon Composites and its Electrochemical Performance in Supercapacitor. *Adv. Energy Mater.* **2011**, *1*, 1101–1108.

(17) Wang, Y. G.; Li, H. Q.; Xia, Y. Y. Ordered Whiskerlike Polyaniline Grown on the Surface of Mesoporous Carbon and Its Electrochemical Capacitance Performance. *Adv. Mater.* **2006**, *18*, 2619–2623.

(18) Fulvio, P. F.; Jaroniec, M.; Liang, C. D.; Dai, S. Polypyrrole-Based Nitrogen-Doped Carbon Replicas of SBA-15 and SBA-16 Containing Magnetic Nanoparticles. *J. Phys. Chem. C* **2008**, *112*, 13126–13133.

(19) Lota, G.; Grzyb, B.; Machnikowska, H.; Machnikowski, J.; Frackowiak, E. Effect of Nitrogen in Carbon Electrode on the Supercapacitor Performance. *Chem. Phys. Lett.* **2005**, *404*, 53–58.

(20) Frackowiak, E.; Lota, G.; Machnikowski, J.; Kierzek, K.; Vix-Guterl, C.; Béguin, F. Optimisation of Supercapacitors Using Carbons with Controlled Nanotexture and Nitrogen Content. *Electrochim. Acta* **2006**, *51*, 2209–2214.

(21) Largeot, C.; Portet, C.; Chmiola, J.; Taberna, P. L.; Gogotsi, Y.; Simon, P. Relation between the Ion Size and Pore Size for an Electric Double-Layer Capacitor. *J. Am. Chem. Soc.* **2008**, *130*, 2730–2731.

(22) Inagaki, M.; Konno, H.; Tanaike, O. Carbon Materials for Electrochemical Capacitors. *J. Power Sources* **2010**, *195*, 7880–7903.

(23) Hulicova-Jurcakova, D.; Seredych, M.; Lu, G. Q.; Bandosz, T. J. Combined Effect of Nitrogen- and Oxygen-Containing Functional Groups of Microporous Activated Carbon on its Electrochemical Performance in Supercapacitors. *Adv. Funct. Mater.* **2009**, *19*, 438–447.

(24) Zhuang, X. D.; Zhang, F.; Wu, D. Q.; Feng, X. L. Graphene Coupled Schiff-base Porous Polymers: Towards Nitrogen-enriched Porous Carbon Nanosheets with Ultrahigh Electrochemical Capacity. *Adv. Mater.* **2014**, *26*, 3081–3086.

(25) Schwab, M. G.; Fassbender, B.; Spiess, H. W.; Thomas, A.; Feng, X. L.; Müllen, K. Catalyst-free Preparation of Melamine-Based Microporous Polymer Networks through Schiff Base Chemistry. *J. Am. Chem. Soc.* **2009**, *131*, 7216–7217.

(26) Ansari, M. B.; Jeong, E. Y.; Park, S. E. Styrene Epoxidation in Aqueous over Triazine-Based Microporous Polymeric Network as a Metal-Free Catalyst. *Green Sust. Chem.* **2012**, *2*, 1–7.

(27) Yang, G. W.; Han, H. Y.; Du, C. Y.; Luo, Z. H.; Wang, Y. J. Facile Synthesis of Melamine-Based Porous Polymer Networks and Their Application for Removal of Aqueous Mercury Ions. *Polymer* **2010**, *51*, 6193–6202.

(28) Morales, S.; Guijarro, F. G.; Ruano, J. L. G.; Cid, M. B. A General Aminocatalytic Method for the Synthesis of Aldimines. *J. Am. Chem. Soc.* **2014**, *136*, 1082–1089.

(29) Song, Y. F.; Li, L.; Wang, Y. G.; Wang, C. X.; Guo, Z. P.; Xia, Y. Y. Nitrogen-Doped Ordered Mesoporous Carbon with a High Surface Area, Synthesized through Organic−Inorganic Coassembly, and Its Application in Supercapacitors. *ChemPhysChem* **2014**, *14*, 2084–2093.

(30) Li, M.; Xue, J. M. Integrated Synthesis of Nitrogen-Doped Mesoporous Carbon from Melamine Resins with Superior Performance in Supercapacitors. *J. Phys. Chem. C* **2014**, *118*, 2507–2517.

(31) Hao, L.; Luo, B.; Li, X. L.; Jin, M. H.; Fang, Y.; Tang, Z. H.; Jia, Y. Y.; Liang, M. H.; Thomas, A.; Yang, J. H.; Zhi, L. J. Terephthalonitrile-Derived Nitrogen-Rich Networks for High Performance Supercapacitors. *Energy Environ. Sci.* **2012**, *5*, 9747–9751.

(32) Schwab, M. G.; Crespy, D.; Feng, X. L.; Landfester, K.; Müllen, K. Preparation of Microporous Melamine-based Polymer Networks in an Anhydrous High-Temperature Miniemulsion. *Macromol. Rapid Commun.* **2011**, *32*, 1798–1803.

(33) Geng, L. L.; Wu, S. J.; Zou, Y. C.; Jia, M. J.; Zhang, W. X.; Yan, W. F.; Liu, G. Correlation Between the Microstructures of Graphite Oxides and Their Catalytic Behaviors in Air Oxidation of Benzyl Alcohol. *J. Colloid Interface Sci.* **2014**, *421*, 71–77.

(34) Wei, H. G.; Zhu, J. H.; Wu, S. J.; Wei, S. Y.; Guo, Z. H. Electrochromic Polyaniline/Graphite Oxide Nanocomposites with Endured Electrochemical Energy Storage. *Polymer* **2013**, *54*, 1820–1831.

(35) Gao, S. Y.; Chen, Y. L.; Fan, H.; Wei, X. J.; Hu, C. G.; Luo, H. X.; Qu, L. T. Large Scale Production of Biomass-Derived N-Doped Porous Carbon Spheres for Oxygen Reduction and Supercapacitors. *J. Mater. Chem. A* **2014**, *2*, 3317–3324.

(36) Saha, U.; Jaiswal, R.; Singh, J. P.; Goswami, T. H. Diisocyanate Modified Graphene Oxide Network Structure: Steric Effect of Diisocyanates on Bimolecular Cross-Linking Degree. *J. Nanopart. Res.* **2014**, *16*, 2404.

(37) He, X. J.; Ling, P. H.; Yu, M. X.; Wang, X. T.; Zhang, X. Y.; Zheng, M. D. Rice Husk-Derived Porous Carbons with High Capacitance by ZnCl₂ Activation for Supercapacitors. *Electrochim. Acta* **2013**, *105*, 635–641.

(38) Xiang, X. X.; Liu, E. H.; Huang, Z. Z.; Shen, H. J.; Tian, Y. Y.; Xiao, C. Y.; Yang, J. J.; Mao, Z. H. Preparation of Activated Carbon from Polyaniline by Zinc Chloride Activation as Supercapacitor Electrodes. *J. Solid State Electrochem.* **2011**, *15*, 2667–2674.

(39) Gavrilov, N.; Pašti, I. A.; Vujković, M.; Travas-Sejdic, J.; Ćirić-Marjanović, G.; Mentus, S. V. High-Performance Charge Storage by N-Containing Nanostructured Carbon Derived from Polyaniline. *Carbon* **2012**, *50*, 3915–3927.

(40) Li, Z.; Xu, Z. W.; Tan, X. H.; Wang, H. L.; Holt, C. M. B.; Stephenson, T.; Olsenab, B. C.; Mitlin, D. Mesoporous Nitrogen-Rich Carbons Derived from Protein for Ultra-High Capacity Battery Anodes and Supercapacitors. *Energy Environ. Sci.* **2013**, *6*, 871–878.

(41) Khai, T. V.; Na, H. G.; Kwak, D. S.; Kwon, Y. J.; Ham, H.; Shim, K. B.; Kim, H. W. Significant Enhancement of Blue Emission and Electrical Conductivity of N-Doped Graphene. *J. Mater. Chem.* **2012**, *22*, 17992–18003.

(42) Li, H. F.; Xi, H. A.; Zhu, S. M.; Wen, Z. Y.; Wang, R. D. Preparation, Structural Characterization, and Electrochemical Properties of Chemically Modified Mesoporous Carbon. *Microporous Mesoporous Mater.* **2006**, *96*, 357–362.

(43) Frackowiak, E.; Beguin, F. Carbon Materials for the Electrochemical Storage of Energy in Capacitors. *Carbon* **2001**, *39*, 937–950.

(44) Sun, G. W.; Long, D. H.; Liu, X. J.; Qiao, W. M.; Zhan, L.; Liang, X. Y.; Ling, L. C. Asymmetric Capacitance Response from the Chemical Characteristics of Activated Carbons in KOH Electrolyte. *J. Electroanal. Chem.* **2011**, *659*, 161–167.

(45) Oh, Y. J.; Yoo, J. J.; Kim, Y. I.; Yoon, J. K.; Yoon, H. N.; Kim, J. H.; Park, S. B. Oxygen Functional Groups and Electrochemical Capacitive Behavior of Incompletely Reduced Graphene Oxides as a Thin-Film Electrode of Supercapacitor. *Electrochim. Acta* **2014**, *116*, 118−128.

(46) Ma, C.; Song, Y.; Shi, J. L.; Zhang, D. Q.; Guo, Q. G.; Liu, L. Preparation and Electrochemical Performance of Heteroatom-Enriched Electrospun Carbon Nanofibers from Melamine Form-aldehyde Resin. *J. Colloid Interface Sci.* **2013**, *395*, 217−223.

(47) Xu, B.; Hou, S. S.; Cao, G. P.; Wu, F.; Yang, Y. S. Sustainable Nitrogen-Doped Porous Carbon with High Surface Areas Prepared from Gelatin for Supercapacitors. *J. Mater. Chem.* **2012**, *22*, 19088−19093.

(48) Lee, Y. H.; Chang, K. H.; Hu, C. C. Differentiate the Pseudocapacitance and Double-Layer Capacitance Contributions for Nitrogen-Doped Reduced Graphene Oxide in Acidic and Alkaline Electrolytes. *J. Power Sources* **2013**, *227*, 300−308.

(49) Wang, G. P.; Zhang, L.; Zhang, J. J. A Review of Electrode Materials for Electrochemical Supercapacitors. *Chem. Soc. Rev.* **2012**, *41*, 797−828.

(50) Zhu, Y. R.; Ji, X. B.; Pan, C. C.; Sun, Q. Q.; Song, W. X.; Fang, L. B.; Chen, Q. Y.; Banks, C. E. A Carbon Quantum Dot Decorated RuO_2 Network: Outstanding Supercapacitances under Ultrafast Charge and Discharge. *Energy Environ. Sci.* **2013**, *6*, 3665−3675.

(51) Lota, G.; Grzyb, B.; Machnikowska, H.; Machnikowski, J.; Frackowiak, E. Effect of Nitrogen in Carbon Electrode on the Supercapacitor Performance. *Chem. Phys. Lett.* **2005**, *404*, 53−58.

(52) Liang, Q. H.; Ye, L.; Huang, Z. H.; Xu, Q.; Bai, Y.; Kang, F. Y.; Yang, Q. H. A Honeycomb-like Porous Carbon Derived from Pomelo Peel for Use in High-Performance Supercapacitors. *Nanoscale* **2014**, *6*, 13831−13837.

(53) Ma, F. W.; Zhao, H.; Sun, L. P.; Li, Q.; Huo, L. H.; Xia, T.; Gao, S.; Pang, G. S.; Shi, Z.; Feng, S. H. A Facile Route for Nitrogen-Doped Hollow Graphitic Carbon Spheres with Superior Performance in Supercapacitors. *J. Mater. Chem.* **2012**, *22*, 13464−13468.

(54) Li, T. T.; Yang, G. W.; Wang, J.; Zhou, Y. Y.; Han, H. Y. Excellent Electrochemical Performance of Nitrogen-Enriched Hier-archical Porous Carbon Electrodes Prepared Using Nano-$CaCO_3$ as Template. *J. Solid State Electrochem.* **2013**, *17*, 2651−2660.

(55) Sun, L.; Tian, C. G.; Fu, Y.; Yang, Y.; Yin, J.; Wang, L.; Fu, H. G. Nitrogen-Doped Porous Graphitic Carbon as an Excellent Electrode Material for Advanced Supercapacitors. *Chem.—Eur. J.* **2014**, *20*, 564−574.

(56) Liu, B.; Shioyama, H.; Jiang, H. L.; Zhang, X. B.; Xu, Q. Metal−Organic Framework (MOF) as a Template for Syntheses of Nanoporous Carbons as Electrode Materials for Supercapacitor. *Carbon* **2010**, *48*, 456−463.